Evaluating Drought Responses of Surface Ozone Precursor Proxies: Variations with Land Cover Type, Precipitation, and Temperature

Jacob G. Naimark[1,2], Arlene M. Fiore[2], Xiaomeng Jin[3], Yuxuan Wang[4], Elizabeth Klovenski[4], and Christian Braneon[5,6]

[1] Columbia College, Columbia University, New York, NY, USA.

[2] Lamont Doherty Earth Observatory, Columbia University, Palisades, NY, USA.

[3] Department of Chemistry, University of California Berkeley, Berkeley, CA USA.

[4] Department of Earth and Atmospheric Sciences, University of Houston, Houston, TX, USA.

[5] NASA Goddard Institute for Space Studies (GISS), New York, NY, USA.

[6] SciSpace, LLC, Bethesda, MD, USA.

Corresponding authors: Jacob G. Naimark (jgn2113@columbia.edu)

Key Points:

- Satellite retrievals of tropospheric NO_2 and HCHO show drought enhancements of 3.5% and 7.7%, respectively, during Eastern US summers
- Low precipitation and high temperatures both independently drive HCHO drought enhancement (10%) in Southeast US woody savannas
- High temperatures drive NO_2 drought enhancement (6.0%) in Midwest US croplands and grasslands

Abstract

Prior work suggests drought exacerbates U.S. air quality by increasing surface ozone concentrations. We analyze 2005-2015 tropospheric column concentrations of two trace gases that serve as proxies for surface ozone precursors retrieved from the OMI/Aura satellite: nitrogen dioxide (ΩNO_2; NO_x proxy) and formaldehyde (ΩHCHO; VOC proxy). We find 3.5% and 7.7% summer drought enhancements for ΩNO_2 and ΩHCHO, respectively, corroborating signals previously extracted from ground-level observations. When we subset by land cover type (using MCD12Q1) and isolate the influences of precipitation and temperature on drought, we find the strongest ΩHCHO drought enhancement (10%) in the woody savannas of the Southeast US. This increase likely reflects biogenic VOC emissions and occurs independently with both high temperature and low precipitation. The strongest ΩNO_2 drought enhancement (6.0%) occurs over Midwest US croplands and grasslands, which we infer to reflect the sensitivity of soil NO_x emissions to temperature.

Plain Language Summary

Projected increases in drought severity and frequency for this century raise questions regarding possible impacts on air quality. Surface ozone, an air pollutant estimated to cause over one million annual premature deaths globally, forms when its precursor gases react in the atmosphere. These precursor gases depend on temperature and precipitation and thus can respond to drought. We analyze over a decade of satellite observations of two trace gases relevant to ozone formation and find that, on average, their concentrations increase during summer droughts in the Eastern US. While we find that higher temperatures during droughts are usually associated with observed increases in trace gas concentrations, in some regions we find increases associated with low precipitation independent of temperature. Satellite detection of these changes implies promise for application to other regions and more generally for improving mechanistic understanding of air quality responses to drought and other climate extremes.

1 Introduction

Surface ozone pollution exacerbates respiratory diseases and has been linked to 1.23 million premature fatalities across the globe annually (Lelieveld et al., 2015; Malley et al., 2017).

Tropospheric ozone production occurs during oxidation of volatile organic compounds (VOCs) as they react with nitrogen oxides (NO_x=NO + NO_2) in the presence of sunlight, and thus peaks during the warm season at mid-latitudes (Sillman et al., 1990). Surface ozone and its precursor gases, NO_x and VOCs, have been found to increase across much of North America during drought (Wang et al., 2017). More severe US droughts are projected for the 21st century due to both lower precipitation and increased evapotranspiration as temperatures rise, with average soil moisture decreasing by up to 12% (Dai, 2013). Below, we exploit over a decade of products retrieved from the Ozone Monitoring Instrument (OMI) aboard the Aura satellite to investigate the implications of drought–parsed separately for the influences of temperature and precipitation–on ozone-related gases during Eastern US summers.

We define drought as an extended period of low precipitation anomalies, which can be exacerbated by high temperatures and increased evapotranspiration, contributing to water-stressed conditions in soil, vegetation, and the atmosphere (Wang et al., 2017). Natural and biogenic NO_x sources, such as soil NO_x, lightning, and wildfires respond to precipitation and temperature, while anthropogenic fossil fuel combustion can be climate-influenced if air conditioning use increases in extreme heat (Abel et al., 2017; Jaeglé et al., 2005; Logan, 1983). Biogenic VOCs (BVOC) emitted from vegetation and wildfires are also linked to temperature and soil moisture and contribute the majority of the global VOC budget (Guenther et al., 2000).

Current satellites do not directly measure near-surface ozone concentrations (Duncan et al., 2014). We use NO_2 and HCHO as proxies for tropospheric NO_x and biogenic VOCs (BVOCs), respectively, the major summertime ozone precursors in the eastern U.S. (e.g., Zhu et al., 2016). Our satellite-based analysis complements a previous study using ground-based measurements, which found a 2-9% increase in NO_2 and a 7-20% increase in isoprene concentrations during drought (Wang et al., 2017). Understanding how ozone precursors respond to drought is relevant for projecting future changes and improving air quality forecasts, and satellite retrievals offer expanded observational coverage to regions lacking ground instruments.

We expect that several processes will enhance ΩNO_2 during drought: (i) soil NO_x pulses following rainfall after an extended low precipitation anomaly, especially in grasslands and croplands (Hudman et al., 2010; Jaeglé et al., 2004; Vinken et al., 2014; Williams et al., 1988; Yienger & Levy II, 1995); (ii) rapid decomposition of PAN during high temperature-driven drought (Sillman & Samson, 1995); (iii) increased lightning frequency during high temperature- and low precipitation-driven drought (Price, 2009); (iv) the use of dirtier power plants during high temperature-driven drought (Abel et al., 2017) and (v) the increase of wildfires during high temperature- and low precipitation-driven drought (Delmas et al., 1995; Koppmann et al., 2005). We expect increases in ΩHCHO from: (i) enhanced leaf foliage emissions of isoprene during droughts with anomalously high temperatures but not extreme water-stress, especially in mixed forests and woody savannas (Brilli et al., 2007; Fortunati et al., 2008; Guenther et al., 1993) and (ii) the increase of wildfires during high temperature- and low precipitation-driven drought (Koppmann et al., 2005; Price, 2009; Singh et al., 2012).

2 Data and Methods

2.1 Eastern US Land Cover Type Classification

We delineate the Eastern US as 23.5 °N to 49.25 °N and -104 °W to -62 °W. We further subdivide this region into the Northeast (37.75 °N to 49.25 °N; -91 °W to -62 °W), Southeast (23.5 °N to 37.75 °N; -91°W to -75.5°W), and Midwest (23.5 °N to 49.25 °N; lon: -104°W to -91°W). We classify land cover types using the NASA Moderate Resolution Imaging Spectrometer (MODIS) MCD12Q1 Land Cover Type product (500 m x 500 m resolution; Friedl & Sulla-Menashe, 2019; Strahler et al., 1999; see Text S1). The most abundant land cover types in each of the three sub-regions of the Eastern US are croplands and grasslands in the Midwest, woody savannas in the Southeast, and mixed forests in the Northeast (see Text S1). We include croplands and grasslands in a single Midwest analysis because their mean ΩNO_2 and ΩHCHO overall drought responses are the same (differences of less than 1.0%).

2.2 OMI/Aura Satellite Retrievals

We use daily ΩNO_2 (available 2005-2017) and ΩHCHO (available 2005-2016) retrievals provided by the QA4ECV product from OMI/Aura (Boersma et al., 2017; De Smedt et al., 2017; Levelt et al., 2006; Zhu et al., 2017), gridded to 0.125° x 0.125° resolution by calculating areaweighted average, as described by Jin et al. (2020). We calculate monthly means from daily observations to reduce noise. To eliminate the influence of small sample sizes, we require at least 10 valid daily measurements to calculate monthly means (see Text S2). We compare drought versus normal conditions in June, July, and August.

2.3 Three Climate Indices: SPEI, SPI, STI

We quantify drought conditions using three climate indices; the Standardized Precipitation Evapotranspiration Index (SPEI), the Standardized Precipitation Index (SPI) and the Standardized Temperature Index (STI), which we develop by adapting the statistical approach used to generate SPI but replacing precipitation with temperature (Fan & van den Dool, 2008; McKee et al., 1993; Zscheischler et al., 2014; see Text S3). Below, we often refer to SPEI as the "overall" drought index or the "P- and T-driven" drought index, while we parse overall drought into "P-driven" drought using SPI and into "T-driven" drought using STI.

SPEI, SPI, and STI quantify climate anomalies on a monthly timescale, relative to long term average conditions at each grid cell. SPEI (0.5° x 0.5° resolution) uses precipitation and evapotranspiration data to classify drought, which effectively incorporates both precipitation and temperature into the index. We use the SPEIbase version 2.5 dataset, which calculates evapotranspiration using the FAO-56 Penman-Monteith equation and incorporates Climate Research Unit Time Series (CRU TS) precipitation and potential evapotranspiration data (University of East Anglia Climatic Research Unit et al., 2017). SPEIbase data are available through 2015 (University of East Anglia Climatic Research Unit et al., 2017; Vicente-Serrano, Beguería, López-Moreno, Angulo et al., 2010; Vicente-Serrano, Beguería, & López-Moreno, 2010), so we restrict drought versus normal analyses to the time period 2005-2015.

SPI incorporates only precipitation data, which makes it simpler to calculate than SPEI, but less indicative of temperature conditions (Keyantash & National Center for Atmospheric Research

Staff, 2018; McKee et al., 1993; see Text S3). We calculate SPI using CRU TS monthly precipitation data interpolated onto a 0.5° x 0.5° resolution grid (University of East Anglia Climatic Research Unit et al., 2020). Similarly, STI incorporates only temperature data, using monthly temperature data from the Global Historical Climatology Network and the Climate Anomaly Monitoring System (GHCN + CAMS) interpolated onto a 0.5° x 0.5° resolution grid (Fan & van den Dool, 2008; see Text S3).

SPEI (0.5 ° x 0.5 °), SPI (0.5 ° x 0.5 °), and STI (0.5 ° x 0.5 °) are converted to match the spatial resolution of the OMI/Aura data (0.125 ° x 0.125 °) by sampling the coarser, original grid cell values that encompass each finer grid cell. MODIS (500 m x 500 m) data are also re-gridded to 0.125 ° x 0.125 ° by sampling the value at the center of each coarser grid cell.

All three climate indices provide location-specific, calendar month-specific deviation values, with a mean of 0 and a standard deviation of 1, enabling comparisons across space and time. We define overall drought conditions as the 10% driest months (SPEI < -1.3) as in Wang et al. (2017). For P-driven drought, we consider the 10% lowest precipitation months (SPI < -1.3), while for T-driven drought, we consider the 10% highest temperature months (STI > 1.3), both of which must also co-occur with overall drought conditions. We control P-driven and T-driven drought for the other variable to minimize bias in one index due to extreme values in the other. For P-driven drought, we include only SPI monthly values that correspond with the condition $-1.3 \leq STI \leq 1.3$. For T-driven drought, we only include STI values for which $-1.3 < SPI < 1.3$. For all drought classifications, SPEI values between -0.5 and 0.5 correspond with normal conditions (Wang et al., 2017).

2.4 Statistical Methods

We apply Welch's t-test to assess significance in mean column concentration differences between normal and drought conditions, and an ordinary (Pearson) least-squares linear regressions to understand the correlative relationship between gas concentrations and SPEI, as well as SPI and STI (each controlled for the other index, as described in Section 2.3). When using Welch's t-test to compare overall drought and normal month ΩNO_2 and $\Omega HCHO$, we include only grid cells that experience at least three drought months and at least three normal months in order to ensure spatial consistency between drought and normal month population samples (see Text S4). When analyzing P-driven and T-driven drought in comparison with normal conditions, we use a minimum threshold of one drought and one normal month to maximize use of available data. We also apply linear regressions to individual grid cells to reflect temporal variability. Because linear regressions do not rely on categorical distinctions between drought and normal months, as in the case of Welch's t-test comparisons, we include all data. When we apply linear regressions to ΩNO_2 and ΩHCHO against SPI and STI, as well as to SPI against STI, we use the full period of 2005-2016 (for all ΩHCHO analyses) and 2005-2017 (for all ΩNO_2 and STI v. SPI analyses) to maximize the OMI/Aura sample size.

3 Results & Discussion

3.1 Overall response of HCHO and NO_2 to drought over the Eastern US

In our broad analysis of Eastern US summers (JJA), we find a mean overall drought enhancement of 3.5% (p=0.000) in ΩNO_2 and 7.7% (p=0.000) in ΩHCHO, consistent in sign and magnitude with a previous analysis of ground-level measurements of NO_x and VOCs in North America (Wang et al., 2017; Figure 1a). ΩNO_2 increases on average by 10% (p=0.000) during T-driven drought but changes by -2.4% (p=0.000) for P-driven drought (Figure 1b,c). Similarly, ΩHCHO is enhanced by 15% (p=0.000) during T-driven drought but changes little during P-driven drought (+0.52%, p=0.000; Figure 1b,c). We thus infer that high temperatures, rather than low precipitation, dominate the broad scale drought response signal in the Eastern US. Given the smaller responses to precipitation than temperature, we infer that changes in the wet depositional sink are not the primary driver of enhanced ΩHCHO and ΩNO_2 during drought.

While we infer that ΩNO_2 and ΩHCHO regional drought enhancements predominantly reflect the influence of high temperatures, the magnitude of the T-driven drought enhancement for both ΩNO_2 and ΩHCHO is weaker than when pure high-temperature anomalies (STI > 1.3) are compared to average temperature conditions (-0.5 < STI < 0.5, both normalized for SPI), where the ΩNO_2 enhancement is 16% and the ΩHCHO enhancement is 18% (not shown). This finding suggests that the observed regional drought responses reflect the slight attenuating effect of water-stress on temperature-dependent emissions sources, like soil NO_x and foliar isoprene emissions, rather than a distinct drought signal (Brilli et al., 2007; Yienger & Levy II, 1995).

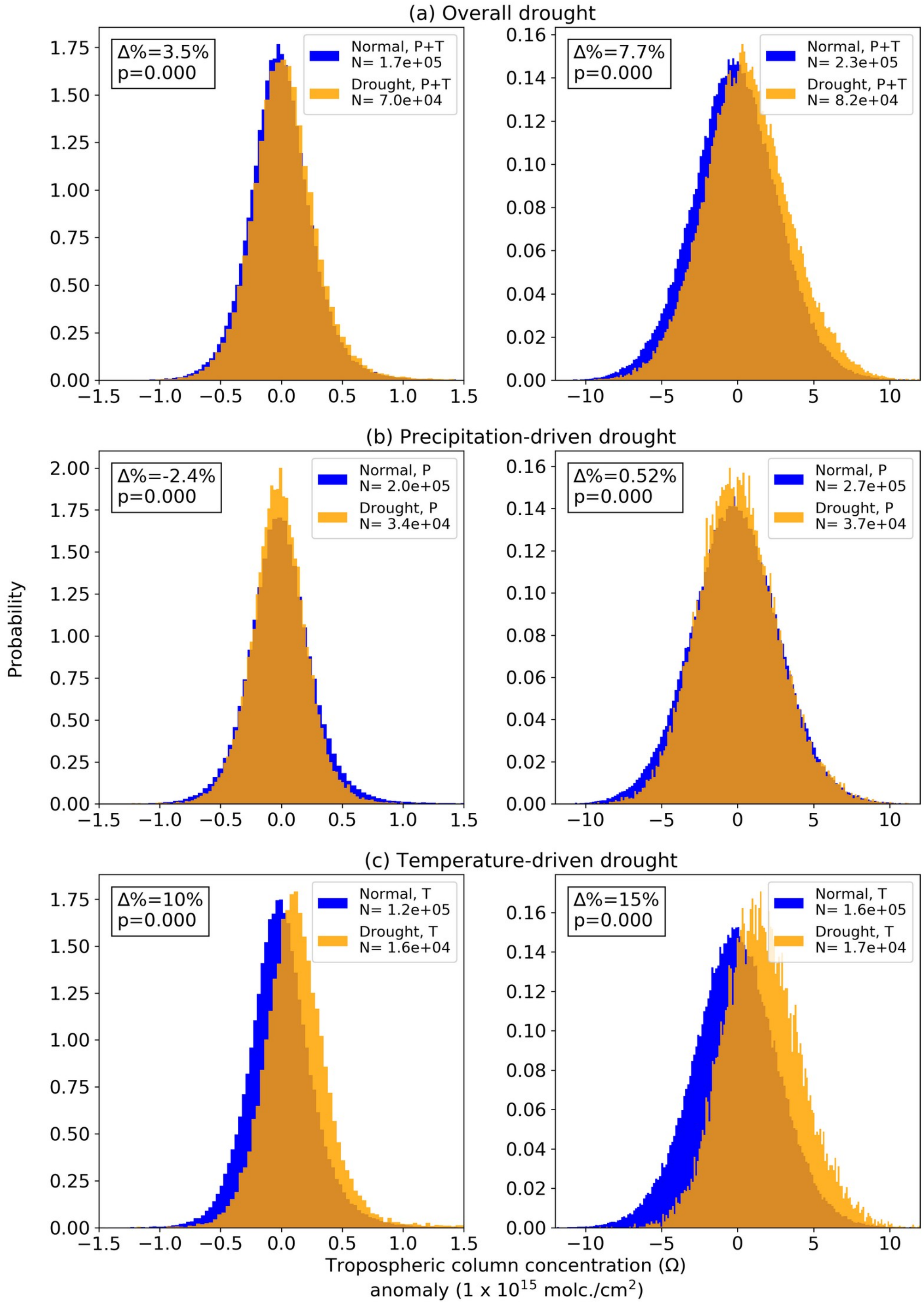

Figure 1: Probability distributions of monthly mean ΩNO_2 (left) and $\Omega HCHO$ (right) anomalies over the Eastern US during June, July, and August, separately for drought (orange) and normal (blue) conditions, where drought is defined as overall drought (1a), precipitation-driven drought (1b), and temperature-driven drought (1c), for 2005-2015. Δ% values represent concentration percentage changes from normal to drought conditions. See Section 2.3 for definitions.

3.2 Drought Response by Land Cover Type

Our finer scale analyses reveal regional variations in ΩNO_2 and $\Omega HCHO$ drought responses (Figure 2a,b,c). ΩNO_2 experiences its strongest overall drought enhancement in the croplands and grasslands of the Midwest US, with a mean enhancement of 6.0% (p=0.000; Figure 3c). For $\Omega HCHO$, the strongest overall drought enhancement occurs in the woody savannas of the Southeast US, with a mean enhancement of 10%, p=0.000 (Figure 4d). Because anthropogenic sources of VOCs contribute only 30% of overall VOC emissions in North America and most anthropogenic sources of NO_x are climate-independent, we infer that sub-regional differences in drought responses are primarily due to variation in natural and biogenic emissions sources (Chen et al., 2019; Wang et al., 2017).

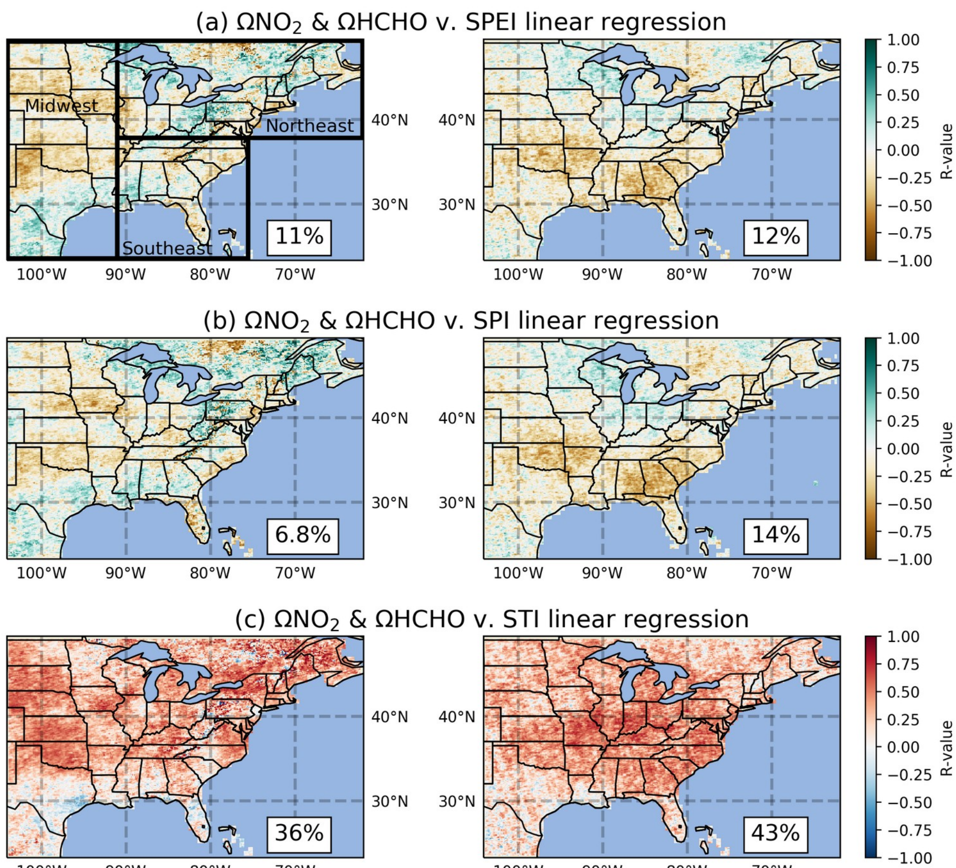

Figure 2: Ordinary least squares (Pearson) correlation of either ΩNO_2 (left) or $\Omega HCHO$ (right) monthly anomalies regressed against SPEI (top, 2a), SPI (middle, 2b), or STI (bottom, 2c) climate indices, over the Eastern US during summer (JJA). SPEI regressions (2a) are for 2005-2015, while SPI (2b) and STI (2c) regressions are for 2005-2016 ($\Omega HCHO$) and 2005-2017 (ΩNO_2). Percentage values in bottom, right corners show the percentage of non-water grid cells in which $p<0.05$.

Additionally, drought occurs less than three times from 2005-2015 in a high portion of grid cells in the Northeast US (see Figure S4). Accordingly, we find only 11% (for NO_2; not shown) and 24% (for HCHO; not shown) of Northeast mixed forests grid cells are represented in our analyses after applying the minimum requirement for number of drought and normal months (see Section 2.4). In the Midwest croplands and grasslands, 46% of grid cells are represented in our analyses (for both NO_2 and HCHO), while in the Southeast woody savannas 62% (for NO_2) and 75% (for HCHO) of grid cells are represented (not shown). Given the limited spatial representation of data in the Northeast mixed forests, we include results for this region only in Supplemental Figure S5, as our sample size limits us from drawing robust inferences.

3.2.1 ΩNO_2

The strong overall ΩNO_2 drought enhancement (6.0%, p=0.000) we observe in the croplands and grasslands of the Midwest mainly reflects a T-driven drought response (+12%, p=0.000), rather than a P-driven drought response (+3.2%, p=0.000; Figure 3c). We infer that this response reflects enhancements in soil NO_x emissions during overall drought, driven by warm, dry conditions during T-driven drought, in light of earlier work indicating a strong, temperature-dependent soil NO_x signal in ΩNO_2 (Hudman et al. 2010; Vinken et al., 2014).

Despite previous findings of pulsing of soil NO_x emissions following rainfall on water-stressed soil (Hudman et al., 2010; Jaeglé et al., 2004; Williams et al., 1988; Yienger & Levy II, 1995), we find only moderate concentration increases during P-driven drought (+3.2%; Figure 3c). The negative correlation between SPI values and ΩNO_2 anomalies (r=-0.12, slope=-0.029, intercept=-0.0069, p=0.000), leads us to infer that water-stressed soil induces microbial rain-pulsing emissions, but that this effect is attenuated due to water-starved soil in the lowest-precipitation months (Figure 3c; Hudman et al., 2010; Yienger & Levy II, 1995). This conclusion is supported by the weak negative correlation between SPI and STI values (r=-0.29, slope=-0.21, intercept=0.21, p=0.000), because higher temperatures during drought months would further amplify rain-pulsing intensity unless, as we infer, water-starved soils inhibit soil NO_x emissions altogether (Figure 3a; Yienger & Levy II, 1995). Irrigation could also potentially explain the diminished effects of rain-pulsing emissions, as it prevents the water-stressed conditions that trigger rain-pulsing events (Yienger & Levy II, 1995).

We infer that the overall ΩNO_2 drought enhancement, as well as the positive correlation between ΩNO_2 anomalies and STI (r=0.33, slope=0.078, intercept=-0.025, p=0.000) observed in the Midwest (Figure 3c) reflects temperature dependent NO_x sources, such as soil NO_x, lightning, fossil fuel combustion, and/or a shorter lifetime of thermally-sensitive NO_x reservoir species, notably peroxy acetyl nitrate (PAN; Abel et al., 2017; Price, 1993; Sillman & Samson, 1995; Yienger & Levy II, 1995). Soil NO_x emissions are strongly temperature dependent, increasing exponentially with temperature in water-saturated soils and roughly linearly in water-stressed soils, and can account for a majority of summer NO_x emissions in croplands and grasslands (Stocker et al., 1993; Yienger & Levy II, 1995). Thus, soil NO_x emissions can increase during T-driven drought, even in the absence of rain-pulsing.

Overall, we find that ΩNO_2 increases during overall drought in areas where soil NO_x emissions comprise a large portion of the total emissions inventory, such as croplands and grasslands (Figure 3c; Vinken et al., 2014; Weng et al., 2020; Williams & Fehsenfeld, 1991). Consistent with this conclusion, the woody savannas of the Southeast US, where soil NOx emissions may be fifty times smaller than in Midwest grasslands (Weng et al., 2020; Williams & Fehsenfeld, 1991; Figure 4c), show little change in ΩNO_2 during overall drought (-0.73%; p=0.021), as well as during P-driven (-1.6%, p=0.0016) and T-driven drought (3.1%, p=0.000; Figure 4c).

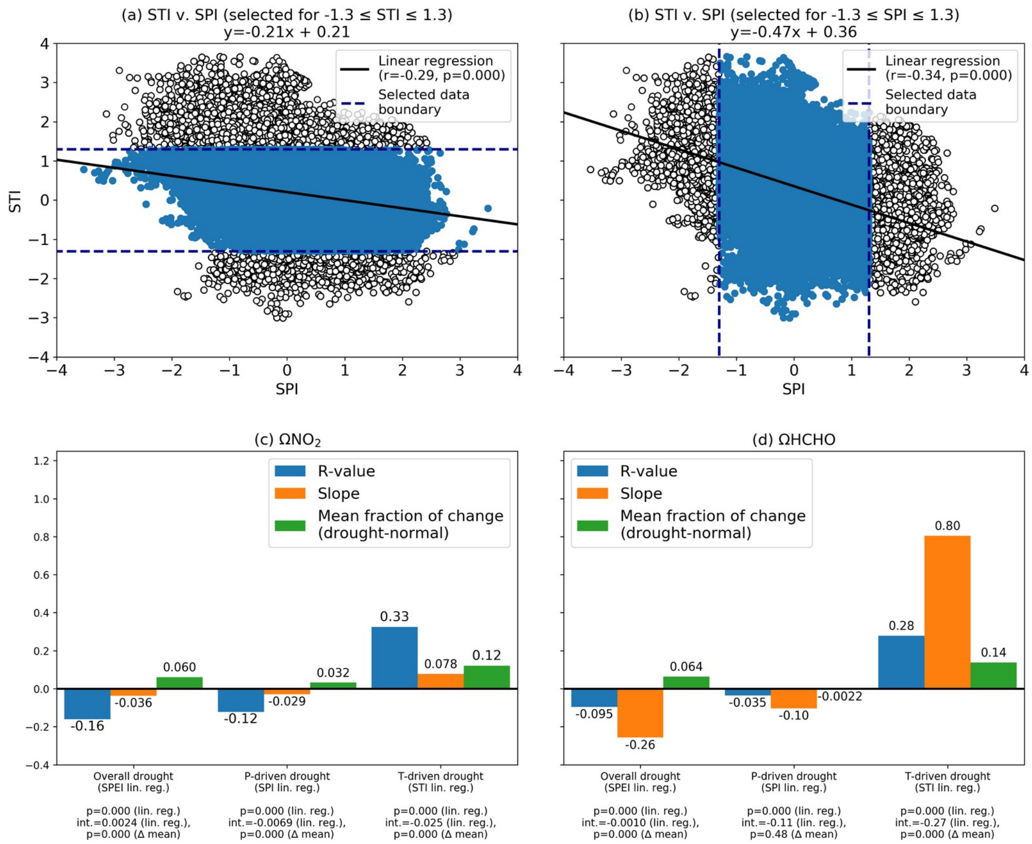

Figure 3: Midwest US croplands and grasslands, drought versus normal conditions comparison. STI is regressed against SPI during June, July, and August of 2005-2017, selecting only grid cells that meet the condition -1.3 ≤ STI ≤ 1.3 (blue points; 3a). STI is also regressed against SPI for the same time period, selecting only grid cells that meet condition -1.3 ≤ SPI ≤ 1.3 (blue points; 3b). Regression line equations are included in titles of 3a and 3b. ΩNO_2 (3c) and ΩHCHO (3d) anomalies in the region are regressed against SPEI, SPI (within selected point range in 3a), and STI (within selected point range in 3b), with r-values (leftmost, blue bars), slopes (middle, orange bars) and p-values and intercepts reported on x-axis tick labels (lin. reg.). SPEI regressions are for 2005-2015, while SPI and STI regressions are for 2005-2016 (ΩHCHO) and for 2005-2017 (ΩNO_2). Mean ΩNO_2 (3c) and ΩHCHO (3d) changes between drought versus normal conditions for overall, P-driven and T-driven drought (all 2005-2015), are reported as fractions (rightmost, green bars), with p-values reported on x-axis tick labels (Δ mean).

3.2.2 ΩHCHO

The strong ΩHCHO overall drought enhancement in the Southeast US woody savannas (+10%, p=0.000) reflects both a P-driven (+7.5%, p=0.000) and T-driven drought response (+9.2%, p=0.000; Figure 4d). Previous findings have established that isoprene emissions, which account for roughly 35% of total BVOC emissions in North America, are enhanced by higher temperatures (Brilli et al., 2007; Guenther et al., 1993, 1995, 2000;). Thus, we infer that the temperature response of BVOC emissions from terrestrial vegetation contributes to the positive correlation between ΩHCHO anomalies and STI values (r=0.41, slope=1.2, intercept=-0.83, p=0.000) and the negative correlation between ΩHCHO anomalies and overall drought index values (r=-0.26, slope=-0.77, intercept=-0.099, p=0.000; Figure 4d).

Prior work suggests extreme water-stress during P-driven drought decreases emissions (Brilli et al., 2007; Fortunati et al., 2008). We find, however, higher ΩHCHO during P-driven drought (+7.5%, p=0.000; Figure 4d), which conflicts with the drying effect of low precipitation on soil moisture decreasing isoprene emissions by up to 25% during moderate water stress and up to 100% when soils are completely water-stressed (Brilli et al., 2007; Fortunati et al., 2008). To our knowledge, increasing VOC emissions with low precipitation and moisture (Figure 4d) has not previously been observed. Though we observe a weak tendency for temperatures to be higher during low precipitation months (r=-0.21, slope=-0.15, intercept=0.23, p=0.000; Figure 4a), this coupled influence is unlikely the dominant factor contributing to the observed 7.5% ΩHCHO enhancement (Fortunati et al., 2008).

An alternative explanation is that higher emissions of monoterpenes, another BVOC, explain the ΩHCHO enhancement during P-driven drought. Monoterpenes are known to be enhanced in water-stressed soils and are about one third as abundant as isoprene during Southeast US summers (Hagerman et al., 1997; Ormeño et al., 2007). Monoterpenes are emitted from certain species at equally high or higher rates during water stress than during average conditions, reflecting heightened carbon use for protection from environmental stressors, such as plant decomposition and insect infestation (Guenther et al., 1995; Ormeño et al., 2007; Pfister et al., 2008; Turtola et al., 2003). During P-driven drought, monoterpenes can protect trees from these threats, causing emissions to increase by nearly 40% in some coniferous species (Turtola et al., 2003). Thus, we infer that this unexpected, but substantial enhancement of ΩHCHO during P-driven drought is predominantly caused by the release of monoterpenes in coniferous vegetation (Guenther et al., 1994; Hagerman et al., 1997; Purves et al., 2004).

HCHO emissions from wildfires during drought could explain a portion of the P-driven drought enhancement (Koppmann et al., 2005; Singh et al., 2012). However, terrestrial vegetation accounts for 98% of BVOC emissions in North America (Guenther et al., 2000), implying a small overall effect of wildfires on total ΩHCHO. A smaller photochemical sink for HCHO during drought could also help explain this result; photolysis seems unlikely to be reduced but drier conditions could reduce loss of HCHO by reaction with hydroxyl radical (OH) if OH production is limited by water vapor abundance (Valin et al., 2016).

The drought response of ΩHCHO in Midwest US croplands and grasslands is entirely dominated by T-driven drought (+14%, $p=0.000$) with no response during P-driven drought ($p=0.48$), and an overall drought enhancement in Midwest croplands and grasslands of +6.4% ($p=0.000$; Figure 3d). These enhancements are consistent with BVOC responses, especially isoprene emissions from terrestrial vegetation in croplands and grasslands (where monoterpenes are expected to contribute little to the overall VOC budget) under warmer temperatures (Bai et al., 2006; Guenther et al., 1995). We infer that the lack of a significant ΩHCHO response to P-driven drought reflects the upward effect of higher temperatures balancing the downward effect of low precipitation on isoprene emissions, given the weak negative correlation between SPI and STI ($r=-0.29$, slope=-0.21, intercept=0.21, $p=0.000$; Figure 3a,d; Fortunati et al., 2008).

Across our study domain, photolysis is a major loss pathway for HCHO. Photolysis is expected to increase during periods with fewer clouds, like drought, intensifying the chemical loss pathway for HCHO (Matthijsen et al., 1998). As such, HCHO emission enhancements during drought may be even stronger than suggested by observed concentration enhancements if higher photolysis shortens the HCHO lifetime during drought.

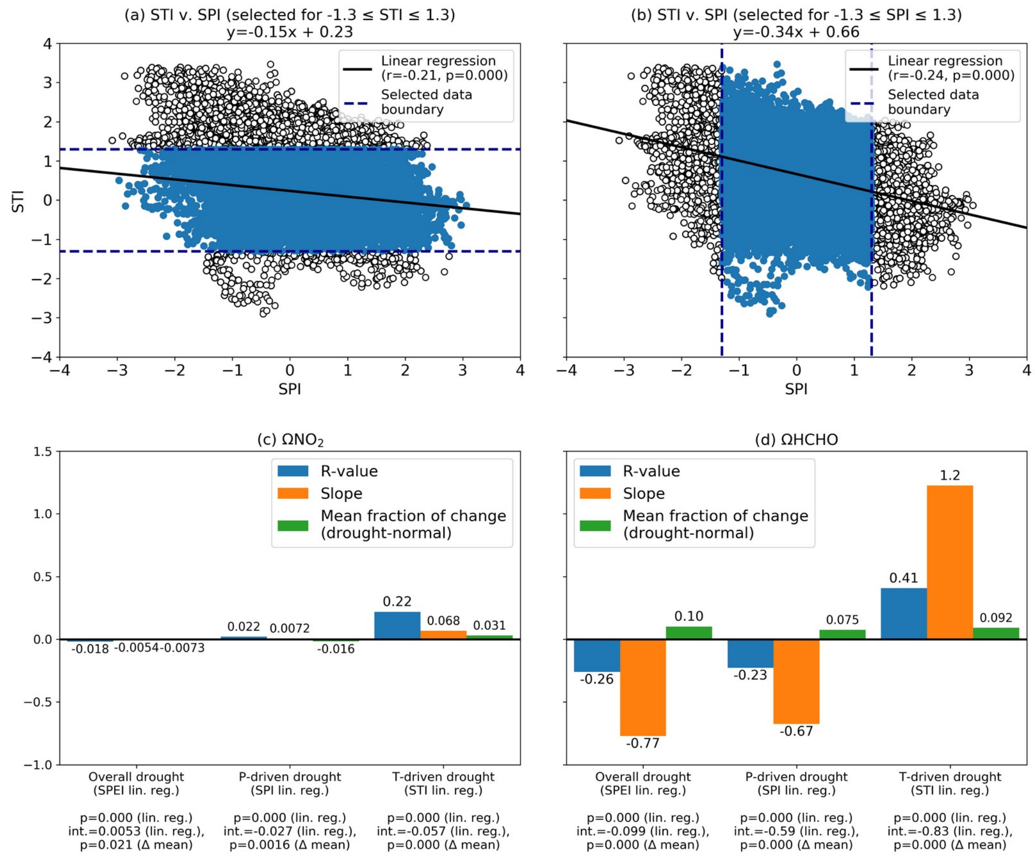

Figure 4: As in Figure 3 but applied to Southeast US woody savannas.

4 Conclusions

The OMI/Aura satellite detects broad scale enhancements in tropospheric columns of NO_2 (ΩNO_2) and HCHO (ΩHCHO) in the Eastern US that are consistent with a previous analysis of ground-based observations in both sign and magnitude (Wang et al., 2017). NO_2 and HCHO drought enhancements are both driven more strongly by high temperatures than by low precipitation. We infer that temperature-driven drought enhancements reflect known emission responses to temperature that occur irrespective of drought.

On finer scales, we find that changes in ΩNO_2 and ΩHCHO depend on the land cover type over which a drought occurs and the extent to which the drought is P-driven versus T-driven. ΩHCHO shows the largest overall drought enhancement in the woody savannas of the Southeast, with a mean enhancement of 10%. This response occurs during both P-driven and T-driven droughts, suggesting that biogenic VOC emissions from terrestrial vegetation can be enhanced even when water stress is unrelated to the influence of high temperature (Guenther et al., 1993; Ormeño et al., 2007; Turtola et al., 2003). We hypothesize that the increase detected in the satellite HCHO product reflects enhanced monoterpene emissions during P-driven drought; this hypothesis could readily be tested with field process studies under drought versus normal conditions.

The ΩNO_2 drought enhancement is largest over Midwest croplands and grasslands, with a mean enhancement of 6.0%. We infer that soil NO_x emissions are predominantly enhanced by T-driven droughts, while surprisingly, the influence of rain pulsing during P-driven droughts does not significantly enhance emissions (Hudman et al., 2010; Vinken et al., 2014; Yienger & Levy II, 1995). Our analysis cannot definitively distinguish the contributions of individual sources or sinks, but future work with models and higher resolution satellite data (e.g., TROPOMI, the upcoming TEMPO; Zoogman et al., 2017; Fletcher & McMullan, 2016) should allow for a more detailed source attribution.

The predicted increase in drought frequency and severity across large regions of the world in the coming century, including the Eastern US, underlines the importance of understanding the effects of drought on air pollution (Dai, 2013). Our use of satellite instruments to detect surface ozone precursor gases could be extended globally to examine the mechanisms driving how pollutants, such as surface ozone, respond to climate extremes like drought.

Acknowledgments

JGN acknowledges Dr. Martin Stute and Dr. Park Williams for contributions to early drafts and SPI MATLAB code, respectively. AMF acknowledges NASA HAQAST NNX16AQ20G and the Vetlesen Foundation; This is LDEO Contribution #.... XJ acknowledges NASA Earth and Space Science Fellowship (NESSF, Grant 80NSSC18K1399). YW acknowledges NASA ACCMAP 80NSSC19K0986.

Data Availability

We downloaded SPEIbase v2.5 from http://dx.doi.org/10.20350/digitalCSIC/8508, which incorporates temperature and potential evapotranspiration data from University of East Anglia Climatic Research Unit et al., 2017 at http://dx.doi.org/10.5285/3df7562727314bab963282e6a0284f24 as described in Vicente-Serrano, Beguería, López-Moreno, Angulo et al., 2010 and Vicente-Serrano, Beguería, & López-Moreno, 2010. We calculated SPI using precipitation data from University of East Anglia Climatic Research Unit et al., 2020 at http://dx.doi.org/10.5285/10d3e3640f004c578403419aac167d82 (see Text S3). We calculated STI using GHCN_CAMS gridded 2m temperature data (see Text S3) provided by the NOAA/OAR/ESRL PSL, Boulder, Colorado, USA at https://psl.noaa.gov/data/gridded/data.ghcncams.html, as described in Fan & van den Dool (2008). We downloaded MODIS MCD12Q1 data described by Friedl & Sulla-Menashe, 2019 from https://doi.org/10.5067/MODIS/MCD12Q1.006. We used the tropospheric column OMI QA4ECV NO_2 product (Boersma et al., 2017) available at http://doi.org/10.21944/qa4ecv-no2-gome2a-v1.1 and HCHO product (De Smedt et al., 2017) available at http://doi.org/10.18758/71021031. We will archive all data and code at Columbia University Academic Commons.

References

Abel, D., Holloway, T., Kladar, R. M., Meier, P., Ahl, D., Harkey, M., & Patz, J. (2017), Response of power plant emissions to ambient temperature in the eastern United States. *Environmental Science & Technology*, *51*(10), 5838–5846. https://doi.org/10.1021/acs.est.6b06201

Bai, J., Baker, B., Liang, B., Greenberg, J., & Guenther, A. (2006), Isoprene and monoterpene emissions from an Inner Mongolia grassland. *Atmospheric Environment*, *40*(30), 5753–5758. https://doi.org/10.1016/j.atmosenv.2006.05.019

Boersma, F., Eskes, H., Richter, A., De Smedt, I., Lorente, A., Beirle, S., et al. (2017), QA4ECV NO2 tropospheric and stratospheric column data from OMI (Version 1.1) [Data set]. *Royal Netherlands Meteorological Institute (KNMI)*. http://doi.org/10.21944/qa4ecv-no2-gome2a-v1.1

Brilli, F., Barta, C., Fortunati, A., Lerdau, M., Loreto, F., & Centritto, M. (2007), Response of isoprene emission and carbon metabolism to drought in white poplar (Populus alba) saplings. *New Phytologist*, *175*, 244–254, https://doi.org/10.1111/j.1469-8137.2007.02094.x

Chen, X., Millet, D. B., Singh, H. B., Wisthaler, A., Apel, E. C., Atlas, E. L., et al. (2019), On the sources and sinks of atmospheric VOCs: an integrated analysis of recent aircraft campaigns over North America. *Atmospheric Chemistry and Physics*, *19*(14), 9097–9123. https://doi.org/10.5194/acp-19-9097-2019

Dai, A. (2013), Increasing drought under global warming in observations and models. *Nature Climate Change*, *3*, 52–28. https://doi.org/10.1038/nclimate1633

Delmas, R., Lacaux, J. P., Menaut, J. C., Abbadie, L., Le Roux, X., Helas, G., & Lobert, J. (1995), Nitrogen compound emission from biomass burning in tropical African savanna FOS/DECAFE 1991 experiment (Lamto, Ivory Coast). *Journal of Atmospheric Chemistry*, *22*, 175–193. https://doi-org.ezproxy.cul.columbia.edu/10.1007/BF00708188

De Smedt, I., Yu, H., Richter, A., Beirle, S., Eskes, H., Boersma, K. F., et al. (2017), QA4ECV HCHO tropospheric column data from OMI (Version 1.1) [Data set]. *Royal Belgian Institute for Space*. http://doi.org/10.18758/71021031

Duncan, B. N., Prados, A. I., Lamsol, L. N., Liu, Y., Streets, D. G., Gupta, P., et al. (2014), Satellite data of atmospheric pollution for U.S. air quality applications: Examples of applications, summary of data end-user resources, answers to FAQs, and common mistakes to avoid. *Atmospheric Environment*, *94*, 647–662. https://doi.org/10.1016/j.atmosenv.2014.05.061

Fan, Y., & van den Dool, H. (2008), A global monthly land surface air temperature analysis for 1948-present. *Journal of Geophysical Research*, *113*(D1). https://doi.org/10.1029/2007JD008470

Fletcher, K., & McMullan, K. (2016), Sentinel 5 Precursor: ESA's Atmospheric Chemistry and Pollution-Monitoring Mission. *European Space Agency*.

Friedl, M., & Sulla-Menashe, D. (2019), MCD12Q1 MODIS/Terra+Aqua Land Cover Type Yearly L3 Global 500m SIN Grid V006 [Data set]. *NASA EOSDIS Land Processes DAAC*. https://doi.org/10.5067/MODIS/MCD12Q1.006

Fortunati, A., Barta, C., Brilli, F., Centritto, M., Zimmer, I., Schnitzler, J., & Loreto, F. (2008), Isoprene emission is not temperature−dependent during and after severe drought−stress: a physiological and biochemical analysis. *The Plant Journal*, *55*(4), 687–697. https://doi.org/10.1111/j.1365-313X.2008.03538.x

Guenther, A., Zimmerman, P. R., Harley, P. C., Monson, R. K., & Fall, R. (1993), Isoprene and monoterpene emission rate variability: Model evaluations and sensitivity analyses. *Journal of Geophysical Research*, *98*(D7), 12609–12617. https://doi.org/10.1029/93JD00527

Guenther, A., Zimmerman, P., & Wildermuth, M. (1994), Natural volatile organic compound emission rate estimates for U.S. woodland landscapes. *Atmospheric Environment*, *28*(6), 1197–1210. https://doi.org/10.1016/1352-2310(94)90297-6

Guenther, A., Hewitt, C. N., Erickson, D., Fall, R., Geron, C., Graedel, T., et al. (1995), A global model of natural volatile organic compound emission. *Journal of Geophysical Research*, *100*(D5), 8873–8892. https://doi.org/10.1029/94JD02950

Guenther, A., Geron, C., Pierce, T., Lamb, B., Harley, P., & Fall, R. (2000), Natural emissions of non-methane volatile organic compounds, carbon monoxide, and oxides of nitrogen from North America. *Atmospheric Environment*, *34*(12–14), 2205–2230. https://doi.org/10.1016/S1352-2310(99)00465-3

Hagerman, L. M., Aneja, V. P., & Lonneman, W. A. (1997), Characterization of non-methane hydrocarbons in the rural southeast United States. *Atmospheric Environment*, *31*(23), 4017–4038. https://doi.org/10.1016/S1352-2310(97)00223-9

Hudman, R. C., Russell, A. R., Valin, L. C., & Cohen, R. C. (2010), Interannual variability in soil nitric oxide emissions over the United States as viewed from space. *Atmospheric Chemistry and Physics*, *10*(20), 13029–13053. https://doi.org/10.5194/acp-10-9943-2010

Jaeglé, L., Martin, R. V., Chance, K., Steinberger, L., Kurosu, T. P., Jacob, D. J., et al. (2004), Satellite mapping of rain-induced nitric oxide emissions from soils. *Journal of Geophysical Research*, *109*(D21), 2007–2023. https://doi.org/doi:10.1029/2004JD004787

Jaeglé, Lyatt, Steinberger, L., Martin, R. V., & Chance, K. (2005), Global partitioning of NOx sources using satellite observations: Relative roles of fossil fuel combustion, biomass burning and soil emissions. *Faraday Discussions*, *130*, 407–423. https://doi.org/10.1039/B502128F

Jin, X., Fiore, A. M., Boersma, K. M., De Smedt, I., & Valin, L. (2020), Changes of summertime surface ozone-NOx-VOC chemistry over U.S. urban areas inferred from two decades of satellite and ground-based observations. *Environmental Science & Technology*. https://doi.org/10.1021/acs.est.9b07785

Keyantash, J., & National Center for Atmospheric Research Staff (Eds). (2018), The Climate Data Guide: Standardized Precipitation Index (SPI). Retrieved from https://climatedataguide.ucar.edu/climate-data/standardized-precipitation-index-spi

Koppmann, R., Czapiewski, K. V., & Reid, J. S. (2005), A review of biomass burning emissions, part I: gaseous emissions of carbon monoxide, methane, volatile organic compounds, and nitrogen containing compounds. *Atmospheric Chemistry and Physics*, *5*, 10455–10516. https://doi.org/10.5194/acpd-5-10455-2005

Lelieveld, J., Evans, J. S., Fnais, M., Giannadaki, D., & Pozzer, A. (2015), The contribution of outdoor air pollution sources to premature mortality on a global scale. *Nature*, *525*, 367–371. https://doi.org/10.1038/nature15371

Levelt, P. F., van den Oord, G. H. J., Dobber, M. R., Malkki, A., Visser, H., de Vries, J., et al. (2006), The ozone monitoring instrument. *IEEE Transactions on Geoscience and Remote Sensing*, *44*(5), 1093–1101. https://doi.org/10.1109/TGRS.2006.872333

Logan, J. A. (1983), Nitrogen oxides in the troposphere: Global and regional budgets. *Journal of Geophysical Research*, *88*(C15), 10785–10807. https://doi.org/10.1029/JC088iC15p10785

Malley, C. S., Henze, D. K., Kuylenstierna, J. C., Vallack, H. W., Davila, Y., Anenberg, S. C., et al. (2017), Updated Global Estimates of Respiratory Mortality in Adults ≥30Years of Age Attributable to Long-Term Ozone Exposure. *Environmental Health Perspectives*, *125*(8), 087021-1-087021–9. https://doi.org/10.1289/EHP1390

Matthijsen, J., Suhre, K., Rosset, R., Eisele, F. L., Mauldin III, R. L., & Tanner, D. J. (1998), Photodissociation and UV radiative transfer in a cloudy atmosphere: Modeling and measurements. *Journal of Geophysical Research*, *103*(D13), 16665–16676. https://doi.org/10.1029/97JD02989

McKee, T. B., Doesken, N. J., & Kleist, J. (1993), The relationship of drought frequency and duration to time scales. *Proceedings of the 8th Conference on Applied Climatology*, *17*(22), 179–183.

Ormeño, E., Mévy, J. P., Vila, B., Bousquet-Mélou, A., Greff, S., Bonin, G., & Fernandez, C. (2007), Water deficit stress induces different monoterpene and sesquiterpene emission changes in Mediterranean species. Relationship between terpene emissions and plant water potential. *Chemosphere*, *67*(2), 267–284. https://doi.org/10.1016/j.chemosphere.2006.10.029

Pfister, G. G., Emmons, L. K., Hess, P. G., Lamarque, J.-F., Orlando, J. J., Walters, S., et al. (2008), Contribution of isoprene to chemical budgets: A model tracer study with the NCAR CTM MOZART−4. *Journal of Geophysical Research*, *113*(D5). https://doi.org/10.1029/2007JD008948

Price, C. (1993), Global Surface Temperatures and the Atmospheric Electrical Circuit. *Geophysical Research Letters*, *20*(13), 1363–1366. https://doi.org/10.1029/93GL01774

Price, C. (2009), Will a drier climate result in more lightning? *Atmospheric Research*, *91*(2–4), 479–484. https://doi.org/10.1016/j.atmosres.2008.05.016

Purves, D. W., Caspersen, J. P., Moorcroft, P. R., Hurtt, G. C., & Pacala, S. W. (2004), Human−induced changes in US biogenic volatile organic compound emissions: evidence from long−term forest inventory data. *Global Change Biology*, *10*, 1737–1755. https://doi.org/doi:10.1111/j.1365-2486.2004.00844.x

Sillman, S., & Samson, P. J. (1995), Impact of temperature on oxidant photochemistry in urban, polluted rural and remote environments. *Journal of Geophysical Research*, *100*(D6), 11497–11508. https://doi.org/10.1029/94JD02146

Sillman, Sanford, Logan, J. A., & Wofsy, S. C. (1990), The sensitivity of ozone to nitrogen oxides and hydrocarbons in regional ozone episodes. *Journal of Geophysical Research*, *95*(D2), 1837–1851. https://doi.org/10.1029/JD095iD02p01837

Singh, H. B., Cai, C., Kaduwela, A., Weinheimer, A., & Wisthaler, A. (2012), Interactions of fire emissions and urban pollution over California: Ozone formation and air quality simulations. *Atmospheric Environment*, *56*, 45–51. https://doi.org/10.1016/j.atmosenv.2012.03.046

Stocker, D. W., Stedman, D. H., Zeller, K. F., Massman, W. J., & Fox, D. G. (1993), Fluxes of Nitrogen Oxides and Ozone Measured by Eddy Correlation Over a Shortgrass Prairie. *Journal of Geophysical Research*, *98*(D7), 12619–12630. https://doi.org/doi:10.1029/93JD00871

Strahler, A., Muchoney, D., Borak, J., Friedl, M., Gopal, S., Lambin, E., & Moody, A. (1999), MODIS Land Cover Product Algorithm Theoretical Basis Document (ATBD) Version 5.0 MODIS Land Cover and Land-Cover Change. Boston University. Retrieved from https://modis.gsfc.nasa.gov/data/atbd/atbd_mod12.pdf

Turtola, S., Manninen, A.-M., Rikala, R., & Kainulainen, P. (2003), Drought Stress Alters the Concentration of Wood Terpenoids in Scots Pine and Norway Spruce Seedlings. *Journal of Chemical Ecology*, *29*, 1981–1995. https://doi.org/10.1023/A:1025674116183

University of East Anglia Climatic Research Unit, Harris, I. C., & Jones, P. D. (2017), CRU TS3.24.01: Climatic Research Unit (CRU) Time-Series (TS) version 3.24.01 of high-resolution gridded data of month-by-month variation in climate (Jan. 1901- Dec. 2015) [Data set]. *Centre for Environmental Data Analysis*. http://dx.doi.org/10.5285/3df7562727314bab963282e6a0284f24

University of East Anglia Climatic Research Unit, Harris, I. C., & Jones, P. D. (2020), CRU TS4.03: Climatic Research Unit (CRU) Time-Series (TS) version 4.03 of high-resolution gridded data of month-by-month variation in climate (Jan. 1901- Dec. 2018) [Data set]. *Centre for Environmental Data Analysis*. http://dx.doi.org/10.5285/10d3e3640f004c578403419aac167d82

Valin, L. C., Fiore, A. M., Chance, K., & Gonzàlez Abad, G. (2016), The role of OH production in interpreting the variability of CH2O columns in the southeast U.S. *Journal of*

Geophysical Research Atmospheres, *121*(1), 478–493. https://doi.org/10.1002/2015JD024012

Vicente-Serrano, S. M., Beguería, S., & López-Moreno, J. I. (2010), A Multi-scalar drought index sensitive to global warming: The Standardized Precipitation Evapotranspiration Index – SPEI. *Journal of Climate*, *23*(7), 1696–1718. https://doi.org/https://doi.org/10.1175/2009JCLI2909.1

Vicente-Serrano, S. M., Beguería, S., López-Moreno, J. I., Angulo, M., & El Kenawy, A. M. (2010), A New Global 0.5° Gridded Dataset (1901–2006) of a Multiscalar Drought Index: Comparison with Current Drought Index Datasets Based on the Palmer Drought Severity Index. *Journal of Hydrometeorology*, *11*(4), 1033–1043. https://doi.org/http://dx.doi.org/10.1175/2010JHM1224.1

Vinken, G. C. M., Boersma, K. F., Maasakkers, J. D., Adon, M., & Martin, R. V. (2014), Worldwide biogenic soil NOx emissions inferred from OMI NO2 observations. *Atmospheric Chemistry and Physics*, *14*(18), 10363–10381. https://doi.org/10.5194/acp-14-10363-2014

Wang, Y., Xie, Y., Dong, W., Ming, Y., Wang, J., & Shen, L. (2017), Adverse effects of increasing drought on air quality via natural processes. *Atmospheric Chemistry and Physics*, *17*(20), 12827–12843. https://doi.org/10.5194/acp-17-12827-2017

Weng, H., Lin, J., Martin, R., Millet, D. B., Jaeglé, L., Ridley, D., et al. (2020), Global high-resolution emissions of soil NOx, sea salt aerosols, and biogenic volatile organic compounds. *Scientific Data*, *7*(148). https://doi.org/10.1038/s41597-020-0488-5

Williams, E. J., & Fehsenfeld, F. C. (1991), Measurement of soil nitrogen oxide emissions at three North American ecosystems. *Journal of Geophysical Research*, *96*(D1), 1033–1042. https://doi.org/10.1029/90JD01903

Williams, E. J., Parrish, D. D., Buhr, M. P., Fehsenfeld, F. C., & Fall, R. (1988), Measurement of soil NOx emissions in central Pennsylvania. *Journal of Geophysical Research*, *93*(D8), 9539–9546. https://doi.org/10.1029/JD093iD08p09539

Yienger, J. J., & Levy II, H. (1995), Empirical model of global soil−biogenic NO_X emissions. *JGR Atmospheres*, *100*(D6), 11447–11464. https://doi.org/10.1029/95JD00370

Zhu, L., Jacob, D. J., Kim, P. S., Fisher, J. A., Yu, K., Travis, K. R., et al. (2016), Observing atmospheric formaldehyde (HCHO) from space: validation and intercomparison of six retrievals from four satellites (OMI, GOME2A, GOME2B, OMPS) with SEAC4RS aircraft observations over the southeast US. *Atmospheric Chemistry and Physics*, *16*, 13477–13490. https://doi.org/10.5194/acp-16-13477-2016

Zhu, L., Mickley, L. J., Jacob, D. J., Marais, E. A., Sheng, J., Hu, L., et al. (2017), Long-Term (2005-2014) Trends in Formaldehyde (HCHO) Columns Across North America as Seen by the OMI Satellite Instrument: Evidence of Changing Emissions of Volatile Organic Compounds. *Geophysical Research Letters*, *44*(13), 7079–7086. https://doi.org/doi:10.1002/2017GL073859

Zoogman, P., Liu, X., Suleiman, R. X., Pennington, W. F., Flittner, D. E., Al-Saadi, J. A., et al. (2017), Tropospheric emissions: Monitoring of pollution (TEMPO). *Journal of Quantitative Spectroscopy and Radiative Transfer*, *186*, 17–39. https://doi.org/10.1016/j.jqsrt.2016.05.008

Zscheischler, J., Michalak, A. M., Schwalm, C., Mahecha, M. D., Huntzinger, D. N., Reichstein, M., et al. (2014), Impact of large−scale climate extremes on biospheric carbon fluxes: An intercomparison based on MsTMIP data. *Global Biogeochemical Cycles*, *28*(6), 585–600. https://doi-org.ezproxy.cul.columbia.edu/10.1002/2014GB004826